Electronic Supplementary Material (ESI) for Nanoscale Horizons.

Electronic Supplementary Information

Eighteen functional monolayer metal oxides: wide bandgap semiconductors with superior oxidation resistance and ultrahigh carrier mobility

Yu Guo,[ab] Liang Ma,[b] Keke Mao,[bc] Minggang Ju,[b] Yizhen Bai,[a] Jijun Zhao,[*a] and Xiao Cheng Zeng [*bd]

[a]*Key Laboratory of Materials Modification by Laser, Ion and Electron Beams (Dalian University of Technology), Ministry of Education, Dalian, Liaoning 116024, China*

[b]*Department of Chemistry, University of Nebraska–Lincoln, Lincoln, Nebraska 68588, United States*

[c]*School of Energy and Environment Science, Anhui University of Technology, Maanshan, Anhui 243032, China*

[d]*Department of Chemical & Biomolecular Engineering and Department of Mechanical & Materials Engineering, University of Nebraska–Lincoln, Lincoln, Nebraska 68588, United States*

[*]Corresponding authors: zhaojj@dlut.edu.cn (J. Zhao); xzeng1@unl.edu (X. C. Zeng)

S1. Some typical monolayer metal oxides searched based on the CALYPSO program

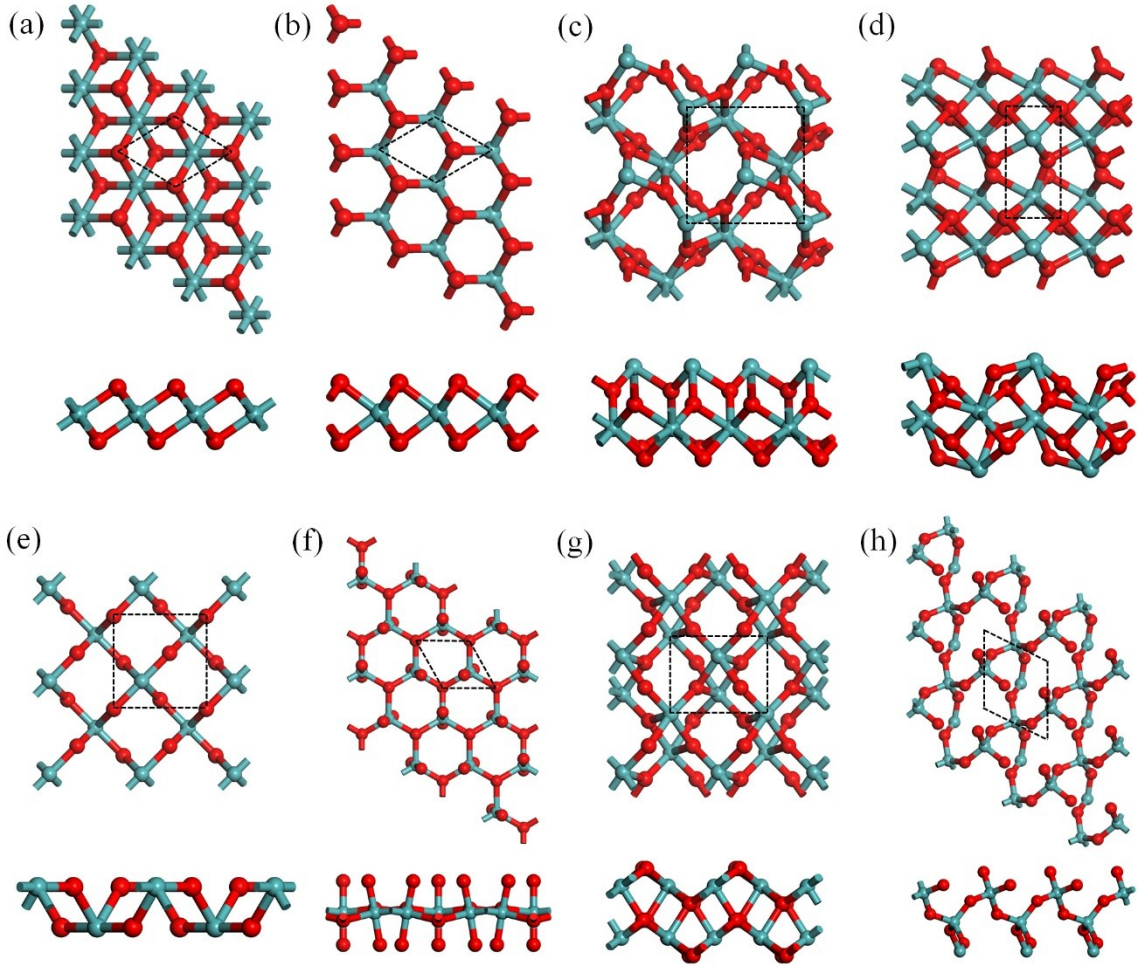

Fig. S1. Some typical freestanding monolayer metal oxides for (a) T phase, (b) H phase, (c) ZrO_2, (d) HfO_2, (e) MoO_2, (f) WO_3, (g) SnO_2 and (h) GeO_2 searched by the CALYPSO program. Metal and O atoms are marked with green and red spheres, respectively. Dashed frames indicate boundaries of primitive cells.

Table S1. Lattice parameters of monolayer metal oxides corresponding to the structures shown in Fig. S1.

Materials	*a* (Å)		Materials	*a* (Å)	
ZrO_2^H	3.16	3.16	TiO_2^H	2.89	2.89
HfO_2^H	3.11	3.11	ZrO_2	5.27	5.42
MoO_2^T	3.17	3.17	HfO_2	5.04	5.07
WO_2^T	2.90	2.90	MoO_2	4.75	4.75
NiO_2^H	2.79	2.79	WO_3	6.12	6.12
PtO_2^H	3.08	3.08	SnO_2	4.79	5.83
GeO_2^H	2.83	2.83	GeO_2	5.09	5.09
TiO_2^T	3.00	3.00			

S2. Convex hull for monolayer metal oxides

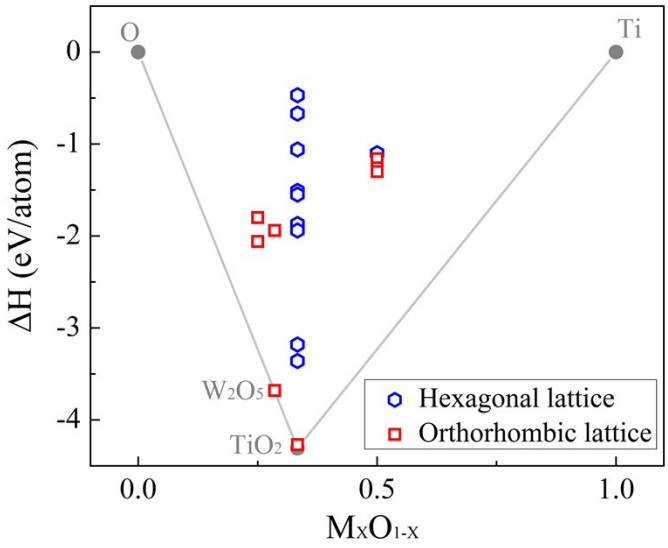

Fig. S2. Convex hull for M_xO_{1-x} (M represents the metal element). The convex hull as defined by the bulk phases is represented by the grey lines. Blue hexagons denote hexagonal phases while red squares represent orthorhombic phases.

S3. Phonon dispersions of monolayer metal oxides

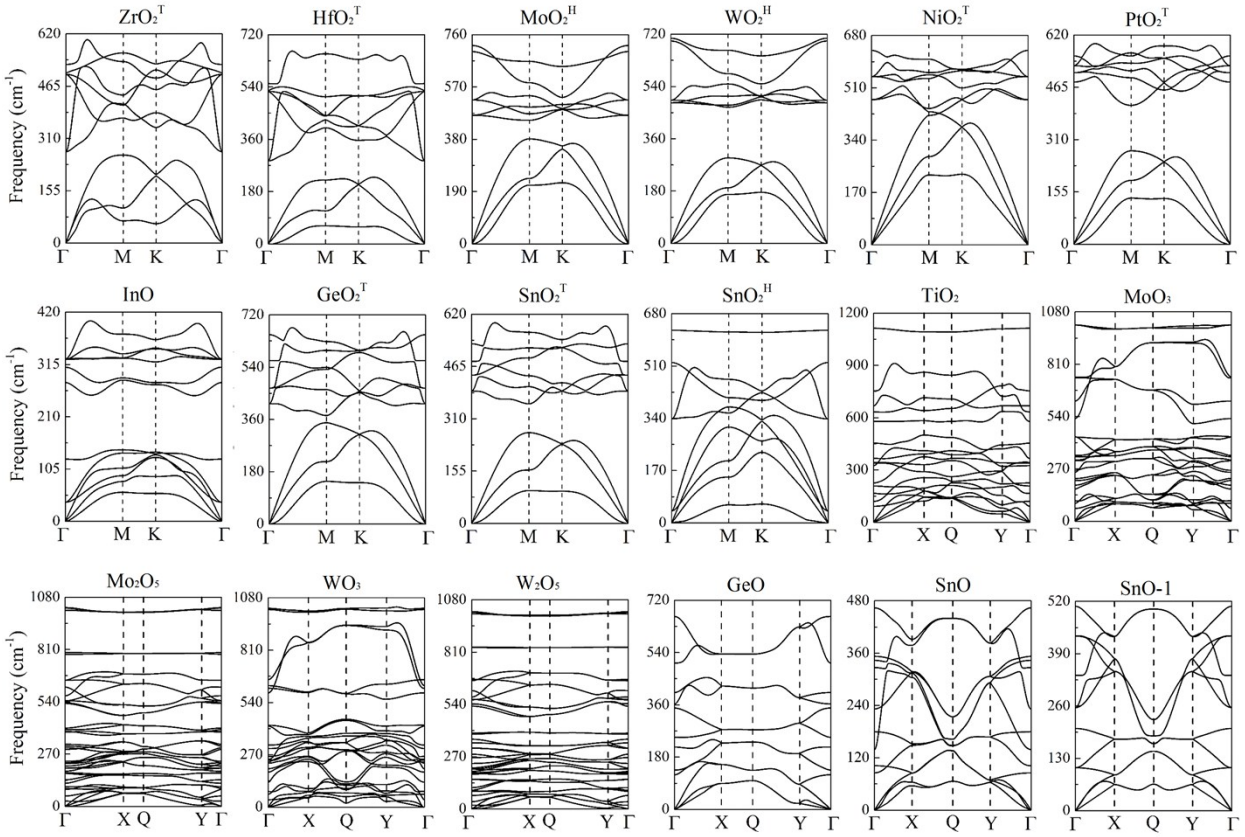

Fig. S3. Computed phonon dispersions of 18 monolayer metal oxides.

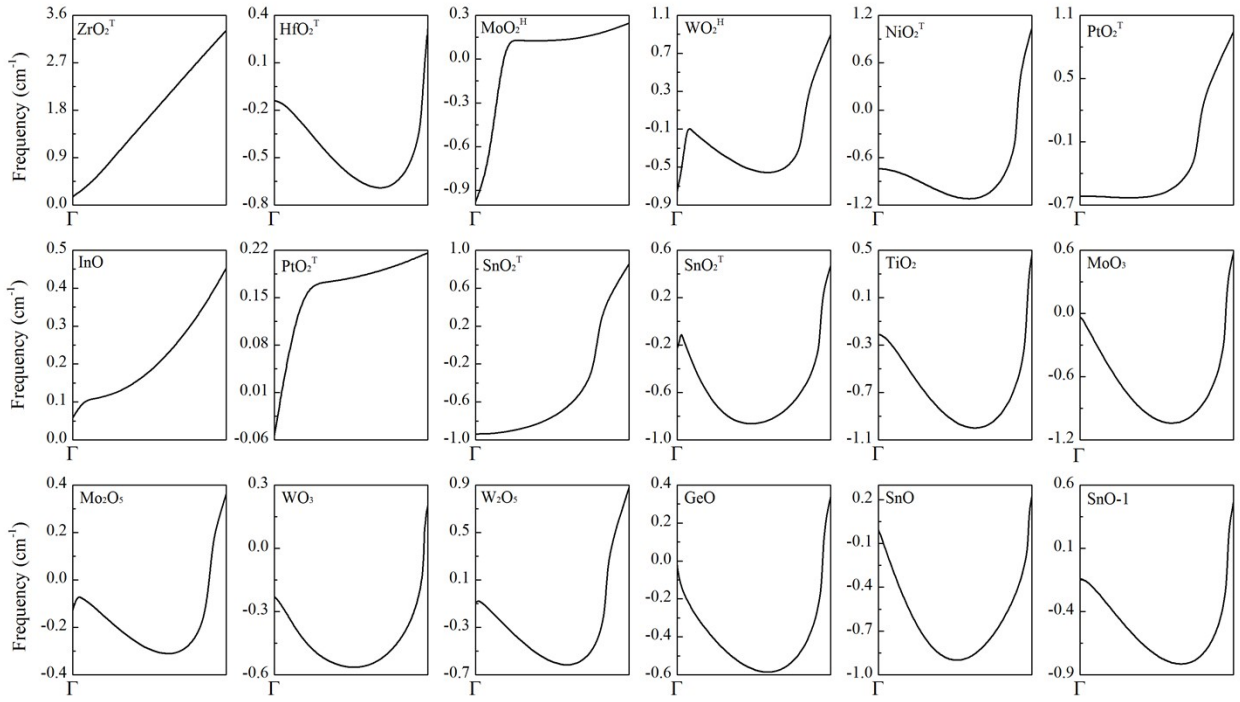

Fig. S4. The phonon dispersion around the gamma point for monolayer metal oxides.

S4. Born-Oppenheimer molecular dynamics (BOMD) snapshots of monolayer metal oxides taken at the end of the simulation. The temperature is controlled at 500 K

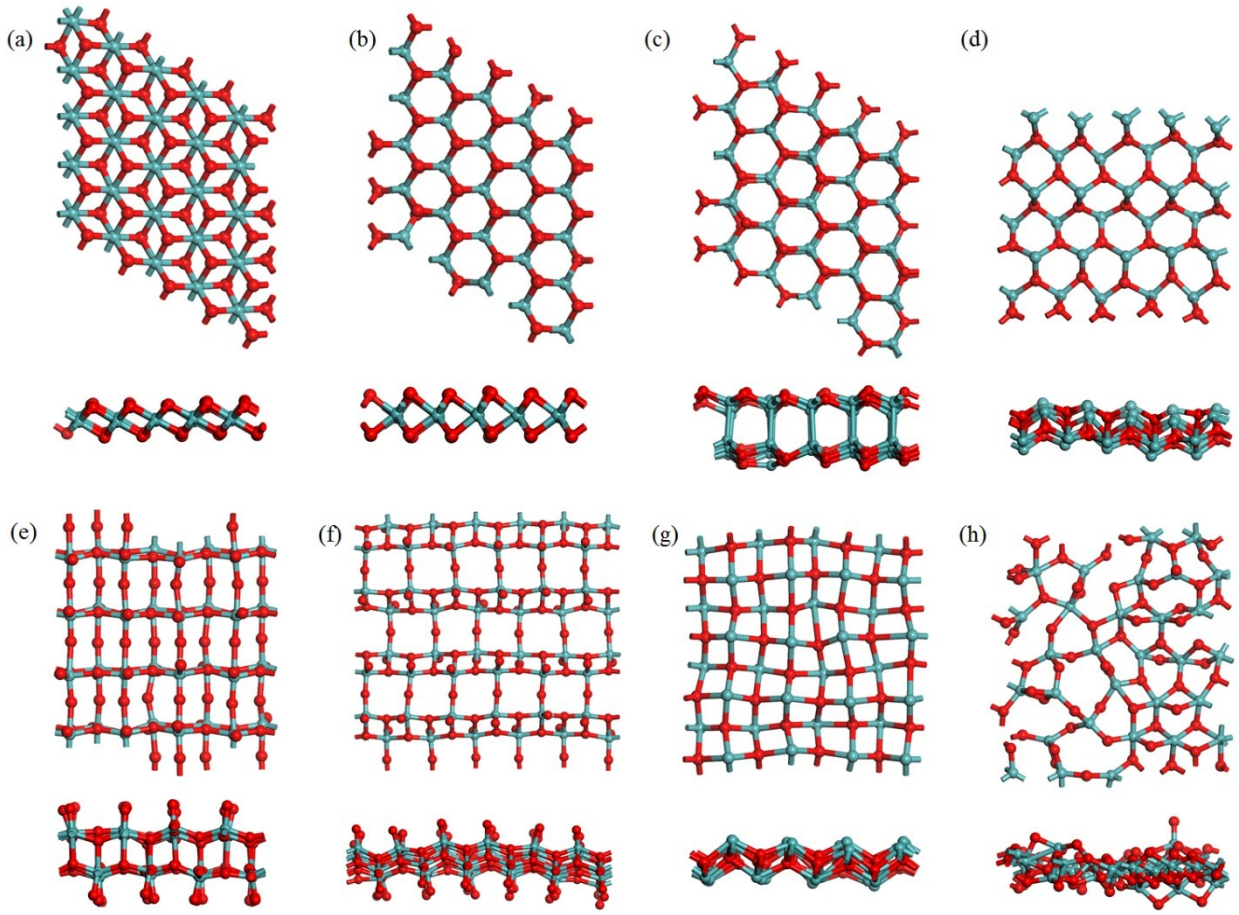

Fig. S5. Snapshots of monolayer structures of (a) ZrO_2^T, HfO_2^T NiO_2^T, PtO_2^T, GeO_2^T, SnO_2^T, (b) MoO_2^H, WO_2^H, SnO_2^H, (c) InO, (d) GeO, SnO, (e) MoO_3, (f) Mo_2O_5, W_2O_5, (g) squared SnO-1 and (h) TiO_2 from BOMD simulations with temperature controlled at 500 K. Each simulation is lasted for 10 ps.

S5. O_2 adsorption on monolayer metal oxides

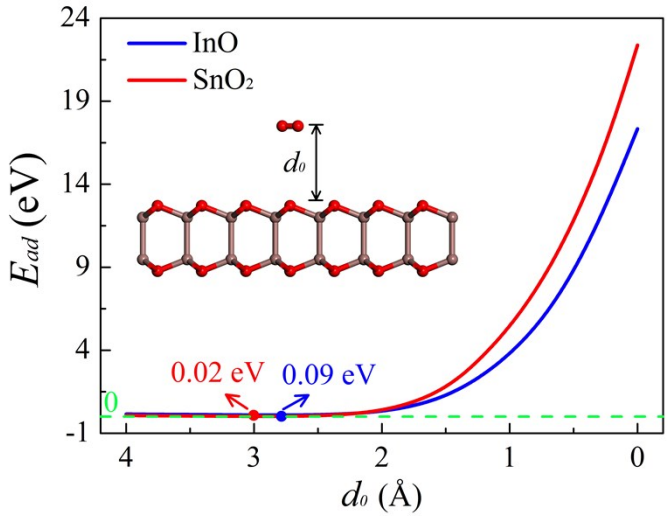

Fig. S6. Computed adsorption energies (E_{ad}) versus d_0, the distance between O_2 and monolayer InO or $SnO_2{}^H$. The green dashed line denotes 0 eV for E_{ad}. The blue and red solid points indicate the location of O_2 physisorption on InO and $SnO_2{}^H$ monolayers, and the blue and red numbers are the O_2 binding energies on InO and $SnO_2{}^H$ monolayer, respectively. By definition, a positive E_{ad} means the endothermic adsorption of O_2 molecule, i.e., unfavorable O_2 adsorption.

S6. Water adsorption and dissociation on the monolayer metal oxides

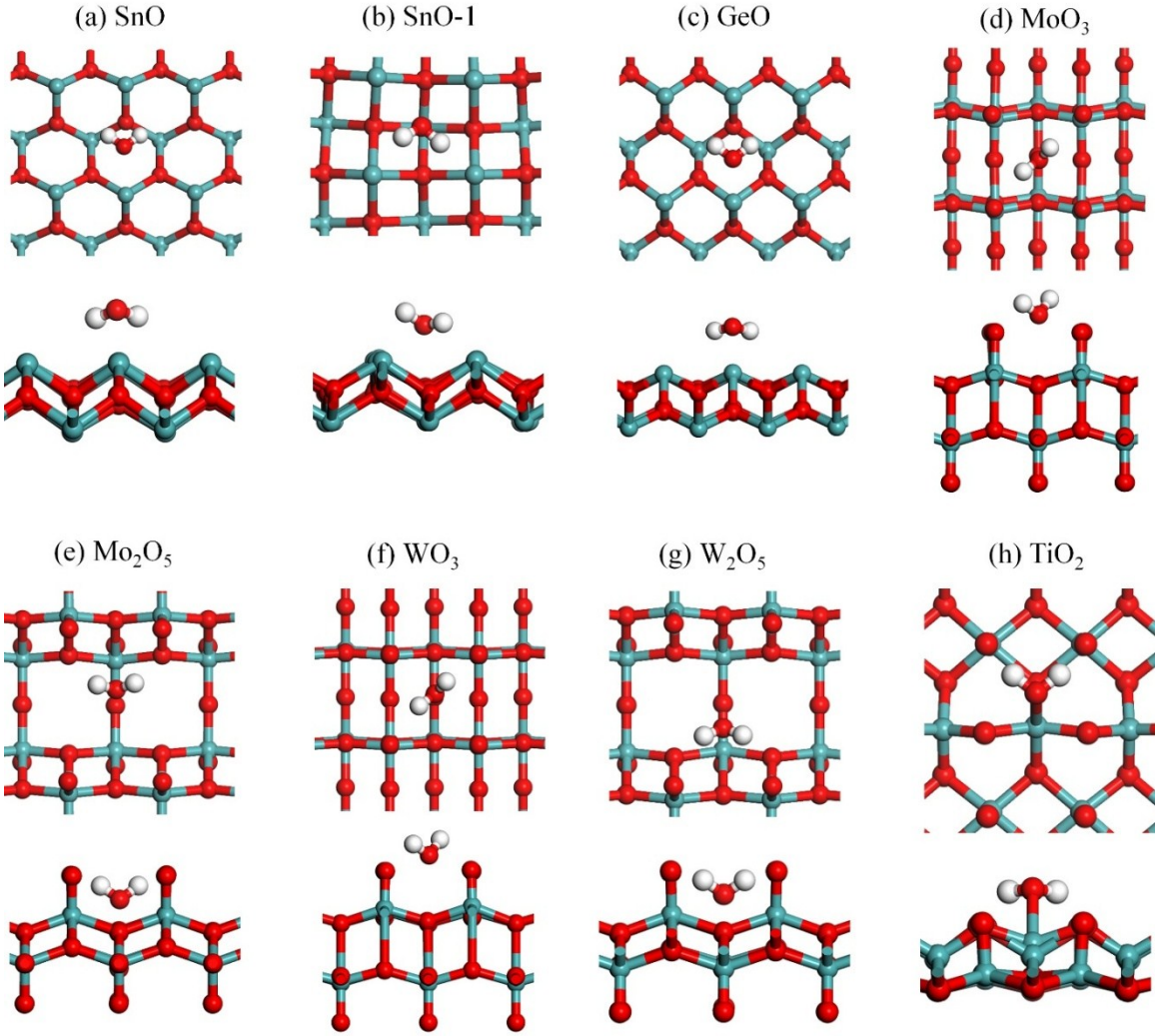

Fig. S7. The atomic structures (top and side views) of H_2O adsorption on monolayer (a) SnO, (b) SnO-1, (c) GeO, (d) MoO_3, (e) Mo_2O_5, (f) WO_3, (g) W_2O_5 and (h) TiO_2. The H, O and metal atoms are shown in white, red and green colors, respectively.

Table S2. The distance (d) between H_2O and these representative monolayers, H_2O adsorption energy E_{ad}^{*1} and dissociated H_2O chemisorption energy E_{ad}^{*2} on monolayers corresponding to the structures in Fig. S7 and Fig. S9, and the reaction of heat (E_H) for H_2O dissociation process.

Monolayers	d (Å)	E_{ad}^{*1} (eV)	E_{ad}^{*2} (eV)	E_H (eV)
SnO	1.63	−0.25	--	--
SnO-1	1.55	−0.28	--	--
GeO	1.73	−0.22	--	--
MoO_3	0.75	−0.17	--	--
Mo_2O_5	--	−0.59	1.04	−1.63
WO_3	0.68	−0.21	--	--
W_2O_5	--	−0.71	1.23	−1.94
TiO_2[1]	1.04	−0.96	−1.52	0.56
TiO_2[2]	1.04	−0.96	3.05	−4.01

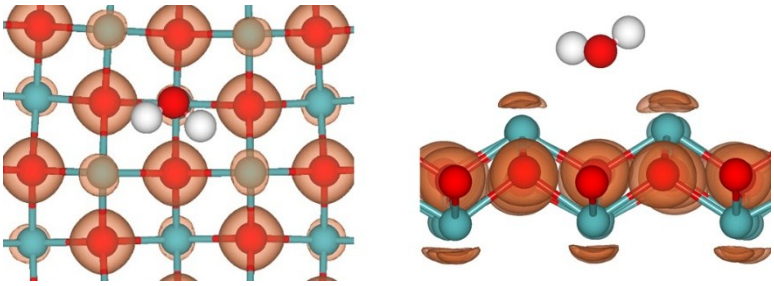

Fig. S8. Differential charge densities of H_2O chemisorption on the SnO-1 monolayer. The H, O and Sn atoms are shown in white, red and green colors, respectively. The orange indicates the electron accumulation with isosurface value of 0.03 |e| per $Å^3$.

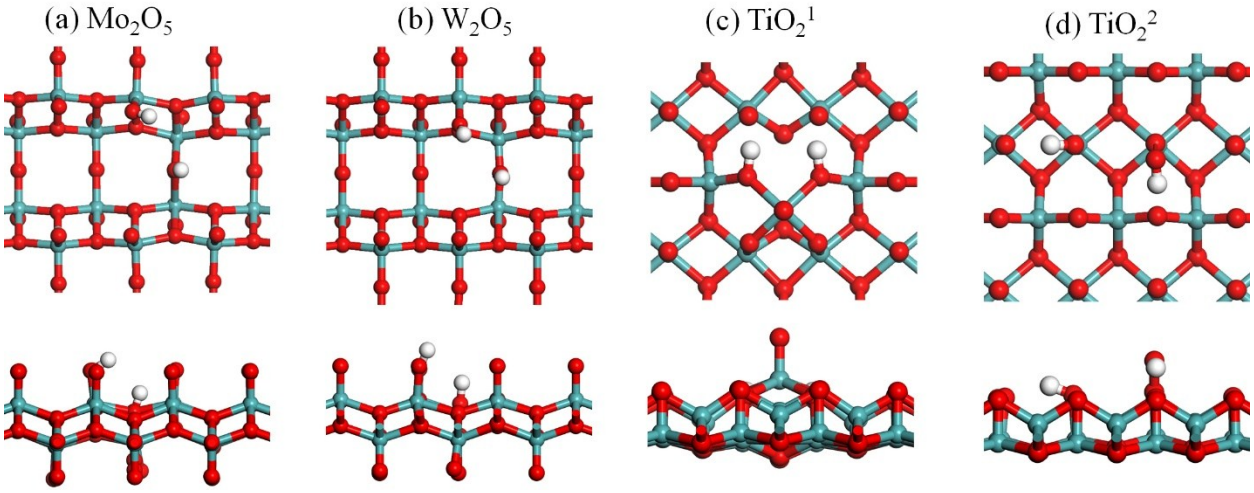

Fig. S9. The atomic structures of H_2O dissociation on monolayer (a) Mo_2O_5, (b) W_2O_5, (c) and (d) TiO_2. The numbers above the structures represent the energy of H_2O chemisorption on the monolayer. TiO_2^1 and TiO_2^2 represent two different configurations of chemisorption. The H, O and metal atoms are shown in white, red and green colors, respectively.

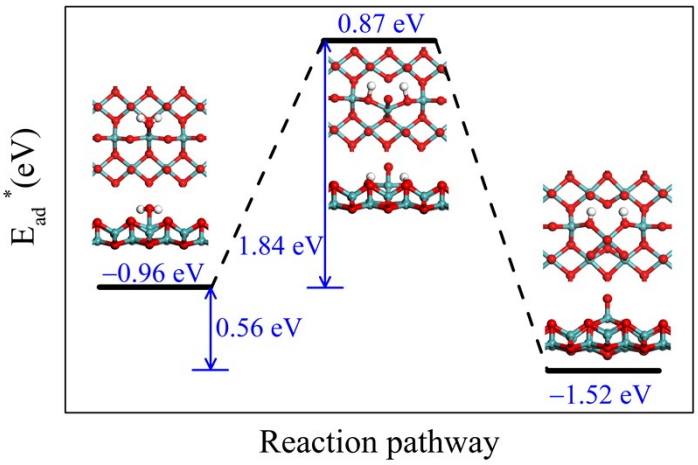

Fig. S10. Reaction pathway for a H_2O molecule to dissociate into two O atoms and an H atom on the TiO2 monolayer. The horizontal black line segments indicate the energy levels of the initial state, transition state, and final state, respectively, with each corresponding atomic structures (top and side views) plotted next to the energy level. The blue numbers (from left to right) represent the binding energy of the initial state, heat of reaction, activation energy, and binding energy of the final state, respectively. The H, O and Ti atoms are shown in white, red and grey colors, respectively.

S7. Monolayer metal oxides as photocatalyst for water splitting

Our computed (HSE06) band structures of MMOs yield a wide range of band gaps from 1.22 to 6.48 eV, most of them exceeding the water redox potential (1.23 eV). In addition to the magnitude of the band gap, the band edges must also straddle the redox potentials of water for possible photocatalytic application. For the water splitting reaction, the redox potential depends on the pH value.[1] The standard reduction potential for H^+/H_2 can be calculated from $E_{H+/H2} = -4.44$ eV + pH × 0.059 eV, while the oxidation potential for O_2/H_2O can be calculated from $E_{O2/H2O} = -5.67$ eV + pH × 0.059 eV. Table 1 presents the computed valence band maximum (VBM) and conduction band minimum (CBM) for each MMOs. For pH = 0 ($E_{H+/H2} = -4.44$ eV and $E_{O2/H2O} = -5.67$ eV), the band edges of TiO_2, GeO, SnO-1, ZrO_2^T and HfO_2^T all straddle the redox potentials of water, suggesting that these layered metal oxides are good candidates as photocatalyst, without the external bias voltage under the acidic environment. Under neutral environment of pH = 7 ($E_{H+/H2} = -4.03$ eV and $E_{O2/H2O} = -5.26$ eV), the band edges of SnO, ZrO_2^T and HfO_2^T satisfy the requirement of water splitting. Overall, the computed band gaps and band-edge positions (HSE06) suggest that several MMOs can be suitable photocatalysts for water splitting. The bare energy required to split water is 1.23 eV. However, additional energy is required to overcome the overpotential for the oxygen and hydrogen evolution processes (OER and HER), and to compensate for the positions of the quasi Fermi levels within the bandgaps.[2] For pH = 0, $E_{H+/H2} = -4.09$ eV and $E_{O2/H2O} = -6.32$ eV, respectively; for pH = 7, $E_{H+/H2} = -3.68$ eV and $E_{O2/H2O} = -5.91$ eV, respectively. Therefore, only GeO monolayer satisfies the bandgap requirement of water splitting. As for the bulk materials, some layered metal oxides have already been proven as promising materials for photocatalytic water splitting in experiments, for instance, layered TiO_2 materials,[3, 4] and WO_3 materials with Mg doping.[5] Encouraged by the findings of these bulk oxide

materials, the functional metal oxide monolayer (or few-layer) materials predicted in this study can be promising candidates for photocatalytic water splitting.

S8. Horizontal/longitudinal anisotropic ratio for carrier effective mass and the longitudinal/horizontal carrier mobility

Table S3. Computed horizontal/longitudinal anisotropic ratio for carrier effective mass, and the longitudinal/horizontal ratio for carrier mobility along *x* and *y* directions. The subscripts *m*, μ, *h* and *e* refer to the carrier effective mass, mobility, hole and electron, respectively.

2D Materials	$R_{m,h}$	$R_{m,e}$	$R_{\mu,h}$	$R_{\mu,e}$
MoO_2^H	1.00	13.30	1.06	115.74
WO_2^H	1.00	18.42	1.20	1.20
NiO_2^T	1.03	1.26	1.22	1.95
PtO_2^T	1.01	6.42	0.05	1.03
InO	1.05	3.30	1.02	0.69
GeO_2^T	1.03	1.00	1.19	1.02
SnO_2^T	2.19	1.00	0.43	1.17
SnO_2^H	0.58	1.00	2.02	1.16
TiO_2	5.07	0.78	0.17	3.92
MoO_3	3.20	1.43	13.76	23.70
Mo_2O_5	1.01	1.17	63.92	85.34
WO_3	1.91	1.40	0.97	1.98
W_2O_5	1.30	1.90	4.33	37.77
GeO	2.27	4.24	1.50	18.60
SnO	0.77	3.71	17.06	8.40
SnO-1	1.00	1.00	1.00	1.00

S9. Strain–total energy relations and shifts of VBM and CBM under strains of monolayer metal oxides

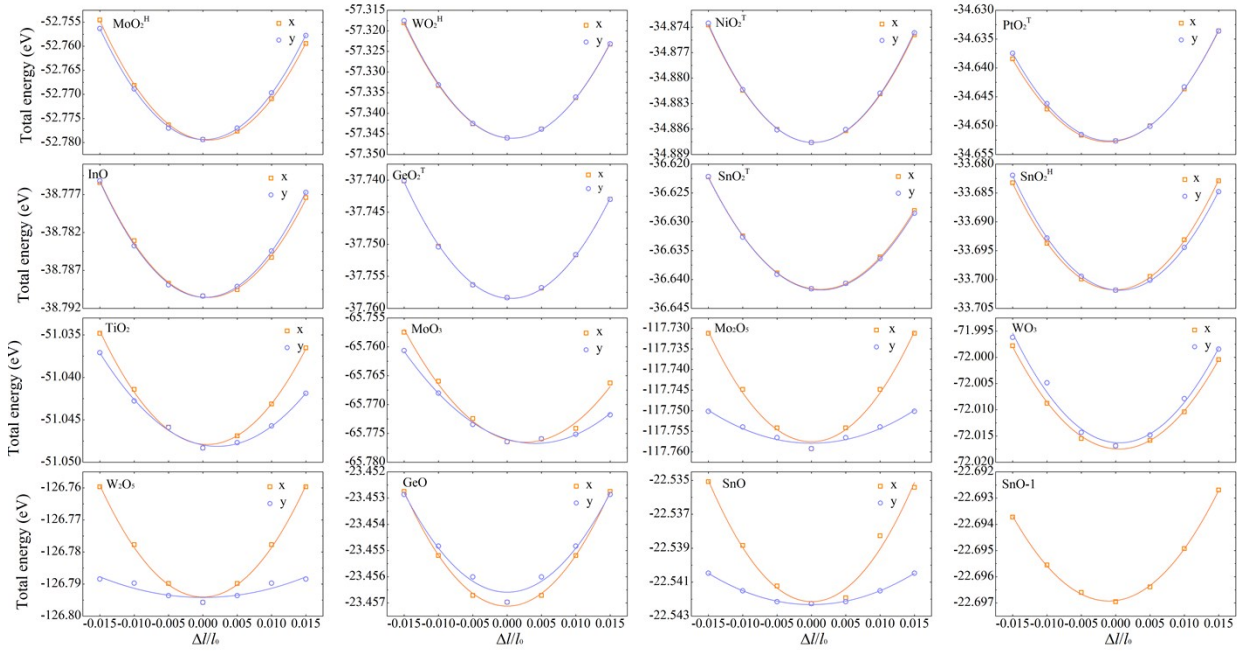

Fig. S11. Strain–total energy relations for monolayer metal oxides.

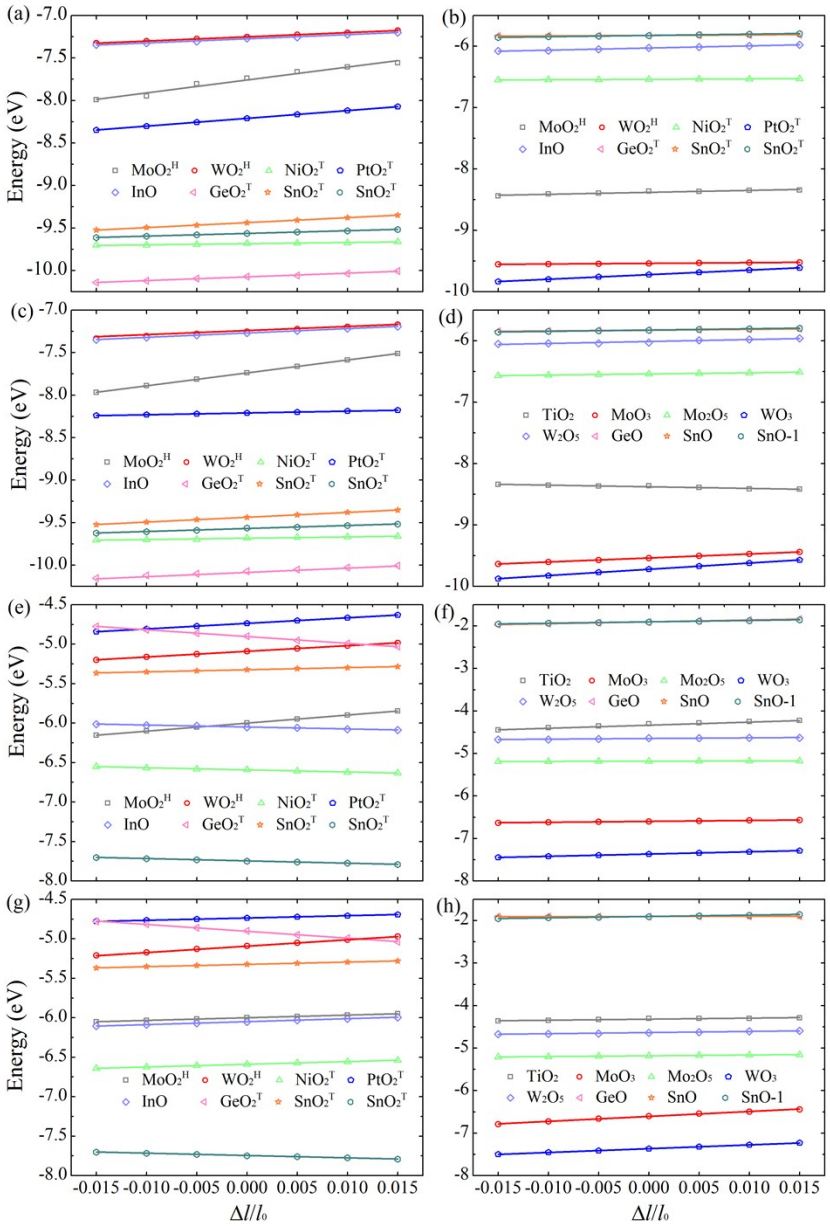

Fig. S12. (a) and (b) Shifts of VBM along *x* direction; (c) and (d) Shifts of VBM along *y* direction; (e) and (f) Shifts of CBM along *x* direction; (g) and (h) Shifts of CBM along *y* direction for monolayer metal oxides. The vacuum level is set at zero for reference.

S10. Electronic properties of selected monolayer metal oxides with including spin-orbit coupling effect

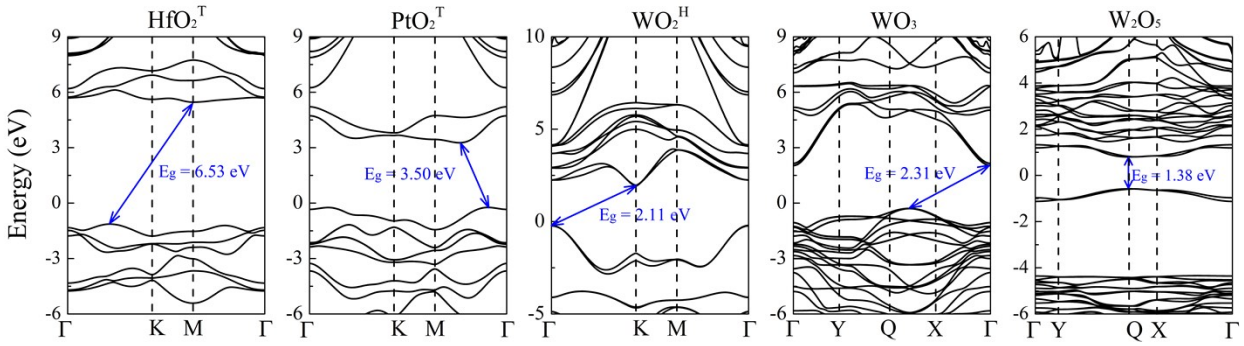

Fig. S13. Electronic band structures of HfO_2^T, PtO_2^T, WO_2^H, WO_3 and W_2O_5 monolayers from left to right panels.

Table S4. Effective mass ratio m^h/m^e of hole/electron carriers, deformation potential constant E_1, elastic modulus C, and hole/electron mobility ratio μ^h/μ^e for selected monolayer metal oxides (with heavy elements like Pt and W considering spin-orbit coupling. m_0 is the electron rest mass. The subscript x and y represent the directions defined in Fig.1.

Hole	m_x^h	m_y^h	E_{1x}	E_{1y}	C_x	C_y	μ_x^h	μ_y^h
	m_0		eV		J•m^{-2}		cm^{2}V^{-1}s^{-1}	
PtO_2^T	1.27	1.30	8.54	2.05	115.56	127.35	20.47	382.44
WO_2^H	0.80	0.80	4.55	5.32	285.47	289.63	454.19	337.07
WO_3	2.82	1.45	7.10	9.98	199.86	200.25	14.66	14.46
W_2O_5	3.84	3.02	3.35	3.17	120.13	20.23	17.26	4.13
Electron	m_x^e	m_y^e	E_{1x}	E_{1y}	C_x	C_y	μ_x^e	μ_y^e
	m_0		eV		J•m^{-2}		cm^{2}V^{-1}s^{-1}	
PtO_2^T	1.00	6.52	6.99	2.80	115.56	127.35	19.53	20.57
WO_2^H	7.10	0.35	7.13	7.80	285.47	289.63	10.58	181.89
WO_3	0.80	0.57	5.26	8.98	199.86	200.25	288.88	136.00
W_2O_5	2.08	3.96	1.60	2.52	120.13	20.23	165.71	5.91

S11. Electronic properties of selected monolayer metal oxides, computed by using DFT+U method

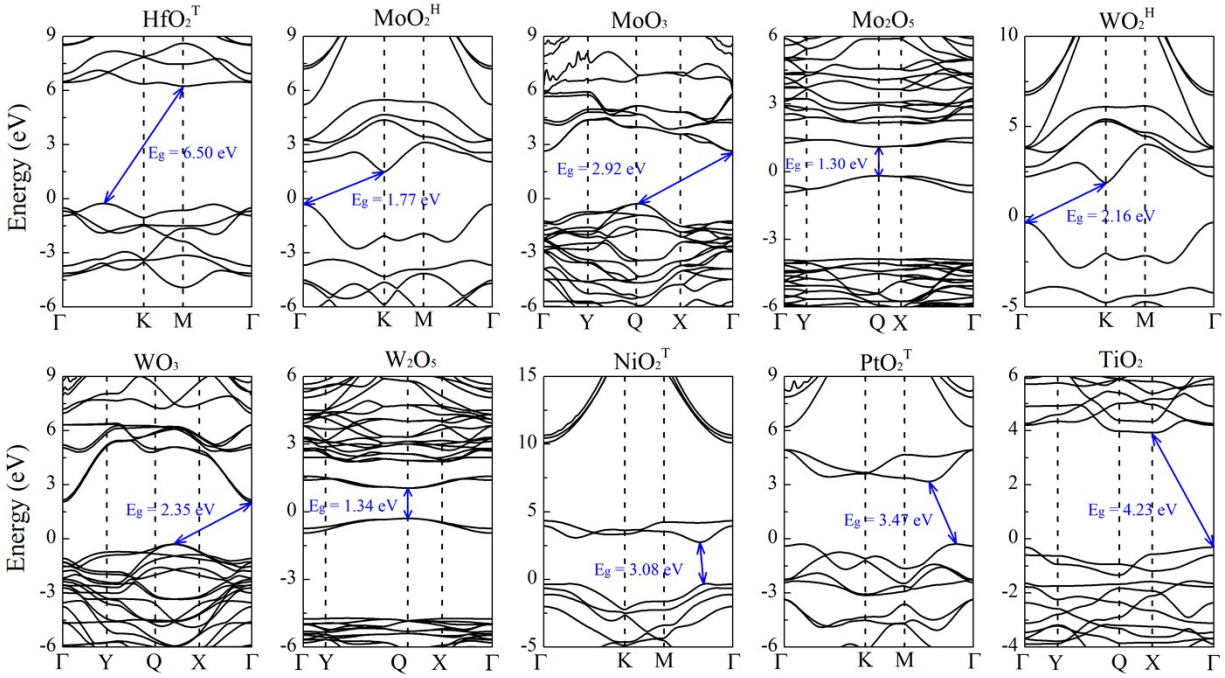

Fig. S14. Electronic band structures of monolayer metal oxides, calculated by using the DFT+U method. The Hubbard U parameters are set as 2.0,[6] 4.8,[7] 6.2,[7] 5.1,[8] 3.0,[8] and 4.2 eV[9] for Hf, Mo, W, Ni, Pt and Ti respectively.

Table S5. Effective mass ratio m^h/m^e of hole/electron carriers, deformation potential constant E_1, elastic modulus C, and hole/electron mobility ratio μ^h/μ^e for monolayer metal oxides using DFT+U method. m_0 is the electron rest mass. The subscript x and y represent the directions defined in Fig. 1.

Hole	m_x^h	m_y^h	E_{1x}	E_{1y}	C_x	C_y	μ_x^h	μ_y^h
	m_0		eV		J•m^{-2}		cm^{2}V^{-1}s^{-1}	
MoO_2^H	0.72	0.72	15.13	15.10	250.25	235.55	44.45	42.01
MoO_3	2.97	0.95	1.14	6.39	179.89	150.81	584.90	48.79
Mo_2O_5	2.26	2.27	0.60	1.85	92.55	12.56	1058.72	15.05
WO_2^H	0.75	0.75	4.90	5.48	286.75	287.69	447.58	359.03
WO_3	2.87	1.49	7.38	10.05	198.32	199.50	12.93	13.51
W_2O_5	3.86	3.15	3.25	3.18	119.05	18.77	7.65	3.56
NiO_2^T	1.89	2.01	1.30	1.53	139.77	145.35	473.28	334.11
PtO_2^T	1.30	1.30	9.01	2.05	120.29	126.46	81.24	375.36
TiO_2	4.44	0.85	3.09	2.61	105.30	84.05	31.91	157.51
Electron	m_x^e	m_y^e	E_{1x}	E_{1y}	C_x	C_y	μ_x^e	μ_y^e
	m_0		eV		J•m^{-2}		cm^{2}V^{-1}s^{-1}	
MoO_2^H	6.15	0.48	10.15	3.25	250.25	235.55	15.13	570.03
MoO_3	0.75	0.53	2.12	11.50	179.89	150.81	328.95	71.94
Mo_2O_5	4.21	3.56	0.52	1.67	92.55	12.56	137.85	6.89
WO_2^H	7.02	0.35	7.10	7.86	286.75	287.69	9.84	178.93
WO_3	0.75	0.55	5.51	8.79	198.32	199.50	179.20	154.09
W_2O_5	2.05	3.85	1.44	2.60	119.05	18.77	116.39	5.41
NiO_2^T	0.70	0.90	2.59	3.29	139.77	145.35	622.35	396.27
PtO_2^T	1.12	6.70	7.00	2.95	120.29	126.46	40.02	16.69
TiO_2	2.39	3.15	7.28	2.48	105.30	84.05	18.75	33.33

S12. Computed carrier mobility of multilayer metal oxides

Table S6. Effective mass ratio m^h/m^e of hole/electron carriers, deformation potential constant E_1, elastic modulus C, and hole/electron mobility ratio μ^h/μ^e for bilayer and trilayer InO. m_0 is the electron rest mass. The subscript x and y represent the directions defined in Figure 1.

Hole	m_x^h	m_y^h	E_{1x}	E_{1y}	C_x	C_y	μ_x^h	μ_y^h
	m_0		eV		J•m^{-2}		cm^{2}V^{-1}s^{-1}	
Bilayer	2.22	1.37	4.80	7.87	195.21	197.56	45.96	28.12
Trilayer	1.78	1.16	6.98	8.75	292.38	266.12	49.59	43.91
Electron	m_x^e	m_y^e	E_{1x}	E_{1y}	C_x	C_y	μ_x^e	μ_y^e
	m_0		eV		J•m^{-2}		cm^{2}V^{-1}s^{-1}	
Bilayer	0.31	0.31	2.37	6.23	195.21	197.56	7489.94	1097.12
Trilayer	0.31	0.31	3.08	2.85	292.38	266.12	6724.84	7242.34

S13. Optical absorption properties of selected monolayer metal oxides

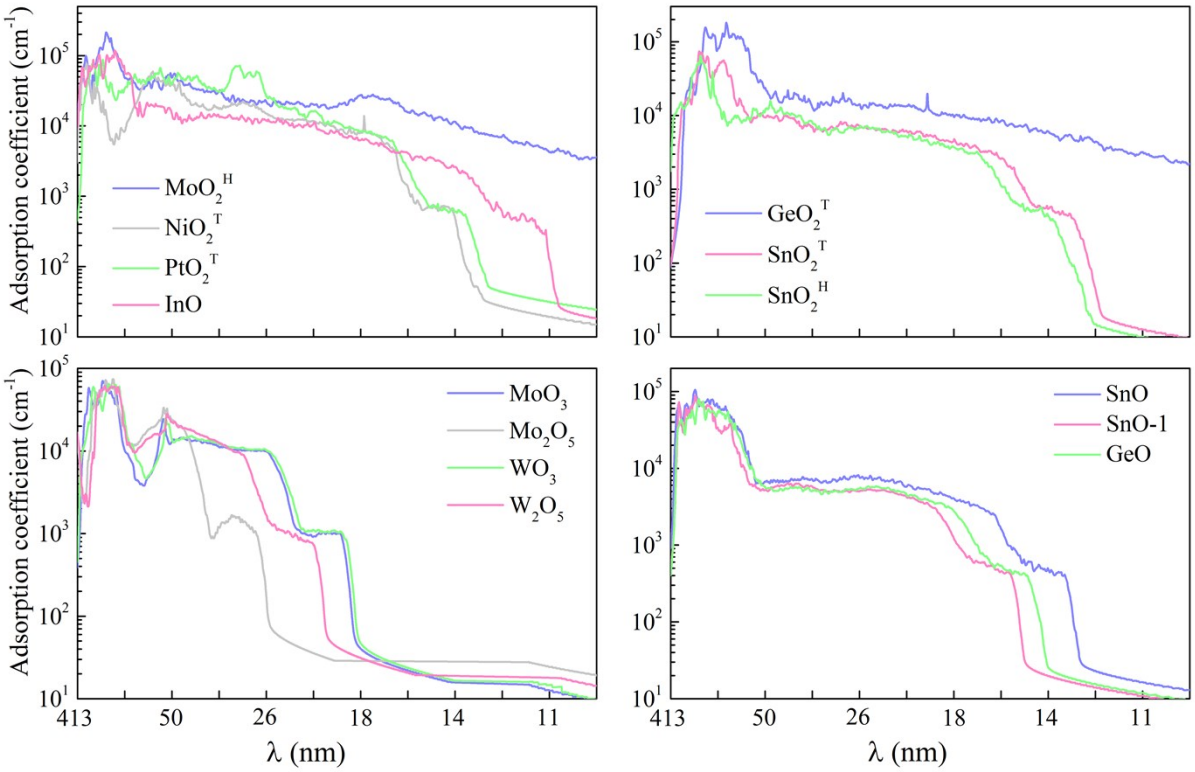

Fig. S15. Computed optical absorption coefficients in ultraviolet wave-length region for selected monolayer metal oxides. λ is the wavelength.

Supplementary References

1 V. Chakrapani, J.C. Angus, A.B. Anderson, S.D. Wolter, B.R. Stoner and G.U. Sumanasekera, *Science*, 2007, **318**, 1424.

2 I.E. Castelli, D.D. Landis, K.S. Thygesen, S. Dahl, I. Chorkendorff, T.F. Jaramillo and K.W. Jacobsen, *Energ. Environ. Sci.*, 2012, **5**, 9034-9043.

3 A. Fujishima, T.N. Rao and D.A. Tryk, *J. Photochem. Photobiol. C-Photochem. Rev.*, 2000, **1**, 1-21.

4 M. Ni, M.K.H. Leung, D.Y.C. Leung and K. Sumathy, *Renew. Sust. Energ. Rev.*, 2007, **11**, 401-425.

5 D.W. Hwang, J. Kim, T.J. Park and J.S. Lee, *Catal. Lett.*, 2002, **80**, 53-57.

6 Y.-F. Zhang, H. Ren and Z.-T. Hou, *J. Magn. Magn. Mater.*, 2015, **375**, 61-64.

7 K. Persson, *https://materialsproject.org/*,

8 Z. Xie, S. Lin and Z. Wang, *Ceram. Int.*, 2018, **44**, 15912-15917.

9 D. Wang, Z.-P. Liu and W.-M. Yang, *ACS Catal.*, 2018, **8**, 7270-7278.